Uniaxial metallo-dielectric metamaterials with scalar positive permeability

Jörg Schilling
Department of Physics, Queen's University Belfast, Belfast, BT7 1NN, United Kingdom
(Received 14 July 2006; published 27 October 2006)

The dispersion relation for plane waves in uniaxial metamaterials with indefinite dielectric tensors and scalar positive permeability is theoretically investigated. It is found, that the isofrequency surfaces of the plane extraordinary waves have a hyperbolic shape which allows the propagation of waves with infinitely long wave vectors. As an example a metallodielectric multilayer was considered and the dispersion relations were determined using an effective medium approximation and an analytically exact Bloch wave calculation. The extraordinary waves in this structure are identified as multilayer plasmons and the validity of the effective medium approximation is examined.

DOI: 10.1103/PhysRevE.74.046618 PACS number(s): 42.70.Qs, 73.20.Mf, 78.67.Pt

INTRODUCTION

Metamaterials for electromagnetic waves are artificial materials which are composed of different elements whose size is much smaller than the wavelength the metamaterial is designed for. The structure on the subwavelength scale leads to new properties for the effective dielectric constant and permeability of the whole metamaterial. In the past the research for metamaterials was mainly concerned with structures which provide a negative refractive index due to simultaneous negative values for dielectric constant ε and permeability μ [1]. Several interesting phenomena were predicted and partly demonstrated for microwaves, e.g., negative refraction [2], subwavelength focusing and imaging [3], and an infinite number of diffraction orders [4]. While the negative value of ε is a natural property of metals and can therefore be incorporated into the metamaterials by simple metallic elements such as metallic rods, the negative value of μ has to be gained using a resonance. For microwave frequencies these resonances can be created using the well known split ring or swiss roll structures. These structures work as *LC* circuits. As negative values of μ can only be achieved sufficiently close to the resonance, the effects relying on a negative μ are only observable in a small frequency range. Furthermore a downscaling of the metamaterials for use in the near infrared and visible range of the electromagnetic spectrum is still difficult, as the size of the *LC* elements has to be reduced well below a micrometer. Therefore simple *LC* elements like closely spaced short rods [5], or small area metal plates [6] were introduced recently which circumvent some of the manufacturing problems.

Here it is suggested that several of the interesting properties for materials with simultaneously negative ε and μ can also be observed in uniaxial anisotropic metamaterials where μ is scalar and positive and only the two principal values of ε have different signs.

The paper is structured in the following way: At first a short review of the wave propagation in uniaxial materials is given and the dispersion relation for ordinary and extraordinary waves is derived followed by a discussion for the specific case of an indefinite dielectric tensor. Afterwards a metallo dielectric multilayer is discussed as an example for a corresponding metamaterial. The propagating modes are investigated applying an effective medium model and exact Bloch wave calculations. This multilayer system is also of practical importance as it was recently suggested for subwavelength imaging [7].

WAVE PROPAGATION IN ANISOTROPIC MEDIA

The optical properties of anisotropic media can be described in form of tensors. As only materials with an anisotropic dielectric constant are considered here, the magnetic permeability μ is scalar and assumed to be $\mu=1$. The dielectric tensor in the coordinate system of the principal axes reads then

$$\hat{\varepsilon} = \begin{pmatrix} \varepsilon_x & 0 & 0 \\ 0 & \varepsilon_y & 0 \\ 0 & 0 & \varepsilon_z \end{pmatrix}. \tag{1}$$

The principal dielectric constants ε_x, ε_y, ε_z depend only on the frequency of the light. Spatial dispersion is not considered in the model.

To simplify further calculations, the principal dielectric constants are assumed to be real. Absorption is therewith neglected. Assuming plane waves of the form $e^{i(\omega t-\vec{k}\cdot\vec{r})}$ for the electric and magnetic fields, the original Maxwell equations $\nabla\times\vec{H}=\dot{\vec{D}}$ and $\nabla\times\vec{E}=-\dot{\vec{B}}$ have the following form:

$$-\vec{k}\times\vec{H} = \omega\varepsilon_0\hat{\varepsilon}\cdot\vec{E} \tag{2}$$

and

$$\vec{k}\times\vec{E} = \mu_0\omega\vec{H}. \tag{3}$$

Combining (2) and (3) results in the following wave equation for the electric field in anisotropic media

$$\frac{1}{\varepsilon_0\mu_0\omega^2}[\vec{k}\times(\vec{k}\times\vec{E})] = -\hat{\varepsilon}\cdot\vec{E}. \tag{4}$$

Using $\vec{k}\times\vec{k}\times\vec{E}=\vec{k}(\vec{k}\cdot\vec{E})-\vec{E}k^2$ and $c^2=\frac{1}{\varepsilon_0\mu_0}$ the following homogeneous system for the components of the electric field, E_x, E_y, E_z, is derived

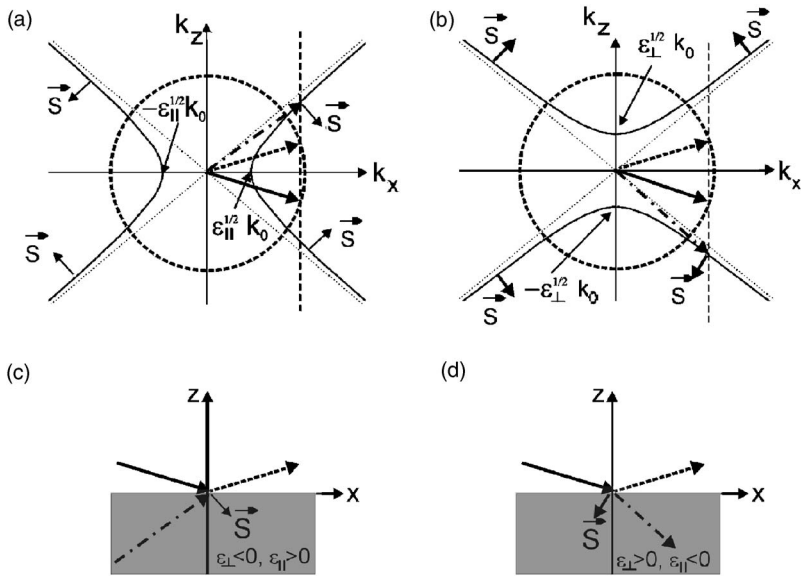

FIG. 1. Diagrams for extraordinary rays and wave vectors in uniaxial media with principal dielectric constants of different sign. (a) Wave vector diagram (k space) for an uniaxial medium with $\varepsilon_{\perp}<0, \varepsilon_{\parallel}>0$. The solid hyperbola represents the wave vectors of all propagating waves in the medium. The long solid arrow identifies the wave vector incident on a xy surface of the medium, while the dashed arrow represents the specular reflected wave vector. The dash-dot arrow is the transmitted wave vector in the uniaxial medium. The short solid arrow indicated with $\vec{S}$ represents the Poynting vector of the transmitted wave. (b) Wave vector diagram (k space) for an uniaxial medium with $\varepsilon_{\perp}>0, \varepsilon_{\parallel}<0$. (c) Waves in real space for $\varepsilon_{\perp}<0, \varepsilon_{\parallel}>0$. (d) Waves in real space for $\varepsilon_{\perp}>0, \varepsilon_{\parallel}<0$.

$$k_x(k_xE_x+k_yE_y+k_zE_z)=\left(k^2-\frac{\omega^2}{c^2}\varepsilon_x\right)E_x,$$

$$k_y(k_xE_x+k_yE_y+k_zE_z)=\left(k^2-\frac{\omega^2}{c^2}\varepsilon_y\right)E_y,$$

$$k_z(k_xE_x+k_yE_y+k_zE_z)=\left(k^2-\frac{\omega^2}{c^2}\varepsilon_z\right)E_z. \tag{5}$$

Nontrivial solutions are obtained by setting the determinant of the system to 0. For the uniaxial materials discussed here, the principal axis is taken along the z direction and the principal dielectric constants are redefined as $\varepsilon_x=\varepsilon_y=\varepsilon_{\perp}$ and $\varepsilon_z=\varepsilon_{\parallel}$. Remembering $k^2=k_x^2+k_y^2+k_z^2$, the resulting equation can be written

$$\left[\frac{\omega^2}{c^2}\varepsilon_{\perp}-k^2\right]\left[\frac{\omega^4}{c^4}\varepsilon_{\perp}\varepsilon_{\parallel}-\frac{\omega^2}{c^2}\varepsilon_{\perp}(k_x^2+k_y^2)-\frac{\omega^2}{c^2}\varepsilon_{\parallel}k_z^2\right]=0. \tag{6}$$

This eigenvalue equation has the following two solutions:

$$\left[\frac{\omega^2}{c^2}\varepsilon_{\perp}-k^2\right]=0 \tag{7}$$

and

$$\left[\frac{\omega^4}{c^4}\varepsilon_{\perp}\varepsilon_{\parallel}-\frac{\omega^2}{c^2}\varepsilon_{\perp}(k_x^2+k_y^2)-\frac{\omega^2}{c^2}\varepsilon_{\parallel}k_z^2\right]=0. \tag{8}$$

Formula (7) determines the dispersion relation for the ordinary waves in the medium. Their electric field is polarized perpendicular to z and they are identical with the E-polarized waves in Ref. [8]. The wavelength $\lambda=2\pi/k$ and with this the refractive index is independent of the direction of the wave vector. Equation (8) is further simplified by setting $k_y=0$ as the choice of the direction of x and y is completely arbitrary within the plane perpendicular to the z axis (xy plane). So (8) becomes

$$\frac{\omega^2}{c^2}=\frac{k_x^2}{\varepsilon_{\parallel}}+\frac{k_z^2}{\varepsilon_{\perp}} \quad \text{or} \quad k_z^2=k_0^2\varepsilon_{\perp}-\frac{\varepsilon_{\perp}}{\varepsilon_{\parallel}}k_x^2, \tag{9}$$

where $k_0=\omega/c$ represents the wave number in vacuum. This is the dispersion relation for the extraordinary waves in the medium. Their magnetic field is polarized perpendicular to z (H-polarized waves in Ref. [8]). For them the wavelength and refractive index depend directly on the direction of the wave vector.

Here we are concerned with materials, whose principal dielectric constants have different signs. The following two cases for uniaxial media with indefinite dielectric tensor exist:

(1) Media with $\varepsilon_{\perp}<0$ and $\varepsilon_{\parallel}>0$.

(2) Media with $\varepsilon_{\perp}>0$ and $\varepsilon_{\parallel}<0$.

In the first case propagating ordinary waves do not exist, as $\varepsilon_{\perp}<0$ and their wave vector is therefore imaginary [see (7)]. In the second case propagating ordinary waves do exist, as $\varepsilon_{\perp}>0$. Because the refractive index for ordinary waves is simply $\sqrt{\varepsilon_{\perp}}$, these waves propagate as in an isotropic medium.

Of much higher interest are the extraordinary waves. In both cases the curve describing the relationship between k_x and k_z (isofrequency curve) forms a hyperbola (Fig. 1). As the hyperbola is unlimited, there exist no maximum k_x or k_z and also the resulting wave number k is unlimited. This means that waves with arbitrary small wavelengths can propagate through the structures.

Let us first concentrate on the special properties of the materials with $\varepsilon_{\perp}<0$ and $\varepsilon_{\parallel}>0$: The isofrequency hyperbola is centered around the x axis and crosses it at $k_x=\pm\sqrt{\varepsilon_{\parallel}}k_0$. This determines the smallest wave vector which can propagate within the structure. When light is incident on the xy surface of the uniaxial material from an isotropic medium above [Fig. 1(c)], it can only be transmitted when its k_x component is larger than $\sqrt{\varepsilon_{\parallel}}k_0$. In Fig. 1(a) the incident wave is represented by the slightly downwards pointing thick solid arrow and its positive k_x component is indicated by the dashed perpendicular construction line. The intersection of

the construction line with the circle determines the specular reflected wave in the isotropic medium while its two intersections with the hyperbola indicate the wave vector within the uniaxial medium for which the k_x component (component parallel to the surface) is conserved. To determine the single transmitted wave, the direction of the Poynting vector $\vec{S}$ of these two preselected waves has to be considered. To obey causality it has to lead away from the surface towards the negative z direction (negative z component of $\vec{S}$). This leaves only the upward wave vector (dash-dot arrow) as transmitted wave. As the Poynting vectors of incident wave and transmitted wave have both positive x components, the wave is refracted in the classical, normal sense. However the opposite z components for incident and transmitted wave vector (incoming wave vector points downwards, while transmitted wave vector points upwards) leads to a backward counting of the phase when the wave travels through the uniaxial medium. This can be used for a compensation of phase similar to what was considered for perfect lenses [3] or compensating bilayers [9].

If the angle of incidence decreases and the k_x component of the incident wave becomes smaller than $\sqrt{\varepsilon_\parallel}k_0$, no intersection between the construction line and the hyperbola can be obtained anymore and all the incident energy is totally reflected. This unusual angle dependency of the total reflection was already found for anisotropic media with partly negative permeability [10]. This can be extended to an omnidirectional total reflection of all waves with all incidence angles, when the refractive index of the upper isotropic medium is smaller than $\sqrt{\varepsilon_\parallel}$. Then the whole wave vector of the incident wave is shorter than $\sqrt{\varepsilon_\parallel}k_0$ and no transmitted wave exists for any angle of incidence.

Let us now consider the media with $\varepsilon_\perp > 0$ and $\varepsilon_\parallel < 0$. Here for every k_x a propagating wave with a real k_z can be obtained and the minimum absolute value of k_z is $\sqrt{\varepsilon_\perp}k_0$ for $k_x=0$. Following the same procedure as in Fig. 1(a), the reflected and transmitted waves can be determined which emerge after incidence of a plane wave on a xy surface. Demanding again a Poynting vector with negative z component, the wave vector of the transmitted wave points now downwards away from the interface. However the x component of the Poynting vector is negative, so that negative refraction occurs. A plane slab of this anisotropic material can therefore focus the light coming from a point source which is placed in an isotropic medium above the slab. This also includes the waves which have an evanescent character in the isotropic medium. They are transformed into propagating waves at the upper surface of a slab of the uniaxial material, travel as propagating waves through the slab and form again evanescent modes at the lower end of the slab. Similar such as for anisotropic media with partly negative permeability [4], the hyperbolic isofrequency curve allows an infinite number of propagating diffraction orders within the uniaxial material if a grating is placed on its xy surface.

These examples show, that many interesting new optical phenomena which were originally discovered for metamaterials with a partly negative permeability, are also present in media with purely positive scalar permeability. The indefinite dielectric tensor is sufficient to create the hyperbolic wave vector relationship for the extraordinary waves, which is the basis for these properties.

AN EXAMPLE FOR $\varepsilon_\perp < 0$ AND $\varepsilon_{II} > 0$—THE METALLO DIELECTRIC MULTILAYER

Effective medium approximation

A simple example for an effective anisotropic metamaterial with $\varepsilon_\perp < 0$ and $\varepsilon_\parallel > 0$ is a periodic multilayer stack of alternating metal and dielectric layers. The surface normal of the layers is parallel to the z axis and the layers extend infinitely within the xy plane. The idea is to make the layers so thin, that the multilayer acts as an effective medium. In this case the following Wiener formulas (or Wiener bounds) should be applicable to calculate the two principal dielectric constants, $\varepsilon_\perp^{\text{eff}}$ and $\varepsilon_\parallel^{\text{eff}}$, for this metamaterial:

$$\varepsilon_\perp^{\text{eff}} = f\varepsilon_{\text{metal}} + (1-f)\varepsilon_{\text{diel}}, \tag{10}$$

$$\frac{1}{\varepsilon_\parallel^{\text{eff}}} = \frac{f}{\varepsilon_{\text{metal}}} + \frac{1-f}{\varepsilon_{\text{diel}}} \quad \text{or} \quad \varepsilon_\parallel^{\text{eff}} = \frac{\varepsilon_{\text{metal}}\varepsilon_{\text{diel}}}{f\varepsilon_{\text{diel}} + (1-f)\varepsilon_{\text{metal}}}. \tag{11}$$

f represents the metal filling factor and is defined as $f = \frac{d_{\text{metal}}}{d_{\text{metal}}+d_{\text{diel}}} = \frac{d_{\text{metal}}}{R}$ where d_{metal} and d_{diel} are the thickness of the metal layer and the dielectric layer, respectively. R is the period of the multilayer. In the following a dielectric constant of $\varepsilon_{\text{diel}}=2.25$ is assumed and the metal is silver [11]. The imaginary part of the dielectric constant of silver is neglected. Figure 2 shows the effective dielectric constants for the spectral region from the near infrared to the UV for the filling factors $f=0.5$ and $f=0.88$. The value $\varepsilon_\perp^{\text{eff}}$ is a smooth continuous function over the whole spectral range starting at positive values for short UV wavelengths and falling quickly to negative values in the visible and beyond. The vacuum wavelengths, where $\varepsilon_\perp^{\text{eff}}$ becomes 0, are $\lambda_0=360$ nm ($f=0.5$) and $\lambda_0=328$ nm ($f=0.88$). In contrary the dispersion of the effective dielectric constant $\varepsilon_\parallel^{\text{eff}}$ shows a clear resonance at $\lambda_{0\text{res}}=359$ nm ($f=0.5$) and $\lambda_{0\text{res}}=643$ nm ($f=0.88$). This resonance occurs when $f\varepsilon_{\text{diel}}+(1-f)\varepsilon_{\text{metal}}=0$. At the short wavelength side of the resonance $\varepsilon_\parallel^{\text{eff}}$ stays negative while at the long wavelength side $\varepsilon_\parallel^{\text{eff}}$ is positive. So for wavelengths above $\lambda_{0\text{res}}=359$ nm ($f=0.5$) and $\lambda_{0\text{res}}=643$ nm ($f=0.88$) the desired case of $\varepsilon_\perp < 0$ and $\varepsilon_\parallel > 0$ is achieved. Close to the resonance $\varepsilon_\parallel^{\text{eff}}$ takes extremely large positive or negative values. How far this simple effective medium model describes the reality of wave propagation in the multilayers has to be examined therefore. In the following an analytical model is applied which yields the exact dispersion relation.

Analytical exact calculation

As the structure consists of plane infinitely extended layers, the boundary conditions for the solutions of the wave equation are simple. When the thickness of the dielectric layers d_{diel} is kept well below $\frac{\lambda}{2} = \frac{\lambda_0}{2\sqrt{\varepsilon_{\text{diel}}}}$ no TE-polarized waves (electric field perpendicular to z) can propagate. Then

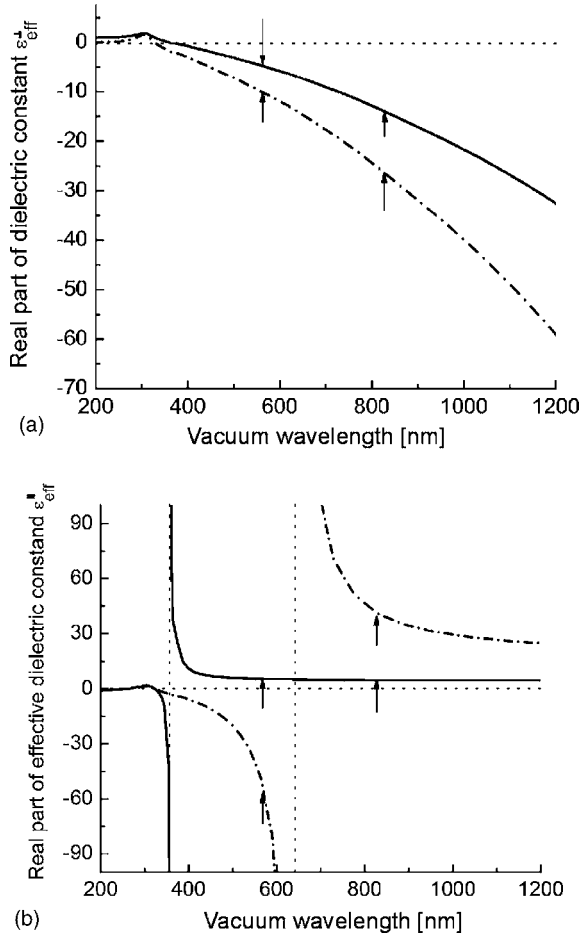

FIG. 2. Effective dielectric constants for multilayer stacks with filling factors of $f=0.5$ (solid) and $f=0.88$ (dash-dot). (a) Dielectric constant perpendicular to $z(\varepsilon_\perp)$. (b) Dielectric constant parallel to $z(\varepsilon_\parallel)$. The small arrows indicate the values of the constants at the specific wavelengths of 563 nm and 826 nm.

indeed only TM polarized waves (magnetic field perpendicular to z) can propagate through the structure. We choose the magnetic field to be oriented along y which leaves $E_x, E_z \neq 0$ and $E_y=0$. The fields in each layer are described as a sum of forward and backward traveling waves. At the interfaces the usual continuity relations for the parallel components of magnetic and electric field are applied [12]. Finally one arrives at a transfer matrix equation which relates the amplitudes of the forward and backward traveling waves in the metal layer of period n ($a^{(n)}_{\text{metal}}$ and $b^{(n)}_{\text{metal}}$) with the amplitudes within the metal layer of period $(n-1)$ ($a^{(n-1)}_{\text{metal}}$ and $b^{(n-1)}_{\text{metal}}$). The transfer matrix equation for the magnetic field amplitudes in the metal layers of adjacent periods reads then

$$\begin{pmatrix} a^{(n-1)}_{\text{metal}} \\ b^{(n-1)}_{\text{metal}} \end{pmatrix} = \begin{pmatrix} A & B \\ C & D \end{pmatrix} \begin{pmatrix} a^{(n)}_{\text{metal}} \\ b^{(n)}_{\text{metal}} \end{pmatrix} \tag{12}$$

with

$$A = e^{ik_{zm}d_{\text{metal}}}\left[\cos k_{zd}d_{\text{diel}} + \frac{1}{2}i\left(\frac{\varepsilon_{\text{diel}}k_{zm}}{\varepsilon_{\text{metal}}k_{zd}} + \frac{\varepsilon_{\text{metal}}k_{zd}}{\varepsilon_{\text{diel}}k_{zm}}\right)\sin k_{zd}d_{\text{diel}}\right],$$

$$B = -e^{-ik_{zm}d_{\text{metal}}}\left[\frac{1}{2}i\left(\frac{\varepsilon_{\text{diel}}k_{zm}}{\varepsilon_{\text{metal}}k_{zd}} - \frac{\varepsilon_{\text{metal}}k_{zd}}{\varepsilon_{\text{diel}}k_{zm}}\right)\sin k_{zd}d_{\text{diel}}\right],$$

$$C = e^{ik_{zm}d_{\text{metal}}}\left[\frac{1}{2}i\left(\frac{\varepsilon_{\text{diel}}k_{zm}}{\varepsilon_{\text{metal}}k_{zd}} - \frac{\varepsilon_{\text{metal}}k_{zd}}{\varepsilon_{\text{diel}}k_{zm}}\right)\sin k_{zd}d_{\text{diel}}\right],$$

$$D = e^{-ik_{zm}d_{\text{metal}}}\left[\cos k_{zd}d_{\text{diel}} - \frac{1}{2}i\left(\frac{\varepsilon_{\text{diel}}k_{zm}}{\varepsilon_{\text{metal}}k_{zd}} + \frac{\varepsilon_{\text{metal}}k_{zd}}{\varepsilon_{\text{diel}}k_{zm}}\right)\sin k_{zd}d_{\text{diel}}\right], \tag{13}$$

where $k_{zm}=\sqrt{\frac{\omega^2}{c^2}\varepsilon_{\text{metal}}-k_x^2}$ and $k_{zd}=\sqrt{\frac{\omega^2}{c^2}\varepsilon_{\text{diel}}-k_x^2}$.

As the multilayer represents a periodic structure along z, its eigenmodes are also Bloch waves and the fields must obey the general phase relation between adjacent periods for Bloch waves. This leads to

$$\begin{pmatrix} a^{(n-1)}_{\text{metal}} \\ b^{(n-1)}_{\text{metal}} \end{pmatrix} = e^{iK_z^B R}\begin{pmatrix} a^{(n)}_{\text{metal}} \\ b^{(n)}_{\text{metal}} \end{pmatrix}. \tag{14}$$

Combining (12) and (14) gives

$$0 = \begin{pmatrix} A - e^{iK_z^B R} & B \\ C & D - e^{iK_z^B R} \end{pmatrix}\begin{pmatrix} a^{(n)}_{\text{metal}} \\ b^{(n)}_{\text{metal}} \end{pmatrix}$$

and setting the determinant to 0 yields the eigenvalue equation for $e^{ik_z^B R}$

$$e^{iK_z^B R} = \frac{A+D}{2} \pm \sqrt{\left(\frac{A+D}{2}\right)^2 - 1}. \tag{15}$$

As we are searching for propagating modes, the Bloch wave number K_z^B has to be real and the absolute value of $e^{iK_z^B R}$ is therefore 1. Close inspection of A and D reveals, that their sum is real ($D=A^*$). In order to obtain a complex number with absolute value 1 on the right hand side of (15) too, it is necessary that $|A+D|\leqslant 2$. Then the square root in (15) is imaginary and the Bloch wave number can be obtained from

$$K_z^B(\omega,k_x) = \frac{1}{R}\arccos\left(\frac{A+D}{2}\right) \pm \frac{2\pi}{R}s \text{ with } s=0,1,2\ldots\ . \tag{16}$$

Here the term $\frac{2\pi}{R}s$ was added to show all possible solutions. This term represents the one dimensional (1D) reciprocal lattice vector and determines the width of the 1D Brillouin zone. From (16) all possible propagating modes with a real K_z^B and their corresponding k_x can be obtained.

Figure 3 shows the resulting dispersion relations. At first a multilayer structure with thin dielectric layers ($d_{\text{diel}}=10$ nm) and thick silver layers ($d_{\text{Ag}}=200$ nm) is investigated [Fig. 3(a)]. The dispersion relation of the multilayer (solid curve) is practically identical with the dispersion of coupled surface plasmons in a single dielectric cavity between bulk silver mirrors. The cavity plasmons form two branches in the dispersion diagram. The lower branch belongs to the cavity plasmons whose magnetic field is symmetric with respect to the center of the cavity while the upper

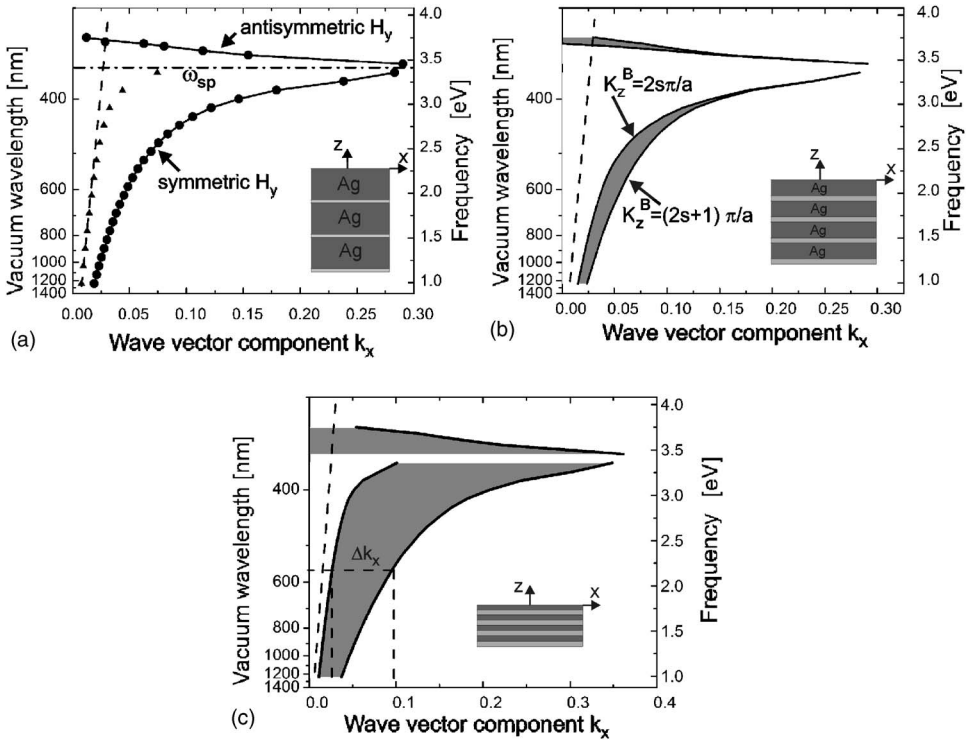

FIG. 3. Development of plasmon bands. The insets show the geometry of the investigated structure. (a) Dispersion relation for a metallodielectric multilayer (solid line) with a thickness of the silver layers $d_{Ag}=200$ nm and a thickness of the dielectric layers of $d_{diel}=10$ nm. The dispersion of coupled plasmons for a single dielectric cavity between two infinitely extended silver mirrors fits very well (circles). For comparison the dispersion relation of surface plasmons at a single dielectric-silver interface (triangles) and the light line in the dielectric (straight dashed line) are shown. The horizontal dash-dot line marks the limiting frequency of surface plasmons at the dielectric-silver interface. (b) Dispersion relation for a metallodielectric multilayer with $d_{Ag}=30$ nm and $d_{diel}=10$ nm. The grey shaded areas are filled with plasmonic modes and represent plasmonic bands. (c) Dispersion relation for a metallodielectric multilayer with $d_{Ag}=10$ nm and $d_{diel}=10$ nm. Increased coupling of the surface plasmons leads to a broadening of the plasmonic bands.

flat branch represents the cavity plasmons with asymmetric magnetic field distribution.

The coupling between the cavity plasmons belonging to different dielectric layers is extremely weak due to the thick separating silver layers. So the dielectric layers in the multilayer stack act as almost independent dielectric cavities and the dispersion is hardly influenced at all by the multiple layer stack. For comparison the dispersion of the simple surface plasmon at a single silver/dielectric interface is also shown [triangles in Fig. 3(a)]. These plasmons can only exist below the limiting frequency ω_{sp} (dash-dot line) and its dispersion curve lies close to the light line (dashed) for longer wavelengths. It bends only at higher frequencies. The symmetric cavity plasmon modes have considerable larger wave vectors, which is a result of the strong coupling between the individual plasmonic oscillations at the opposite silver/dielectric interfaces and is facilitated by the very thin dielectric layer/cavity.

If the thickness of the silver layers is reduced to $d_{AG}=30$ nm ($d_{diel}=10$ nm remains constant), the coupling between the cavity plasmons increases and plasmon bands form. It is now possible to fulfill (16) at each frequency for a range of k_x This is indicated by the grey shaded area in Fig. 3(b). The range of the k_x values for which (16) is fulfilled determines the width Δk_x of the plasmon bands in k_x space. The band limits are formed by the modes whose Bloch wave vectors are $K_z^B=0$, $\pm 2\pi/R,\ldots,$ $2\pi s/R$ and $K_z^B=\pm\pi/R$, $\pm 3\pi/R,\ldots,$ $(2s+1)\pi/R$ [solid curves in Fig. 3(b)]. The bandwidth Δk_x still decreases for frequencies close to ω_{sp}. As k_x increases strongly in this spectral region, the fields decay more rapidly perpendicular to the interfaces within the silver. This reduces the coupling across the silver layers and the bandwidth shrinks to almost 0 as in Fig. 3(a) before.

Is the thickness of the silver layers further reduced to $d_{Ag}=10$ nm ($d_{diel}=10$ nm) the coupling of the cavity plasmons across the now very thin silver layers becomes strong and the plasmon bandwidth increases considerably [Fig. 3(c)]. This is especially true for frequencies closer to ω_{sp}. Now the silver layers are thin enough so that even for higher k_x the bandwidth is large. As an example the bandwidth at a vacuum wavelength of 563 nm is determined [Fig. 3(c)]. The band limits lie at $k_x^{bottom}=0.026$ nm^{-1} and $k_x^{top}=0.095$ nm^{-1} and the bandwidth is $\Delta k_x=k_x^{top}-k_x^{bottom}=0.069$ nm^{-1}. With this the k_x-component of the wave vector at the upper band edge is about 5.6 times larger than the wave number in the dielectric at the same frequency ($k_{diel}=0.017$ nm^{-1}).

This evolution of plasmon bands suggests, that the TM polarized waves traveling through a metallodielectric multilayer can be identified as coupled surface plasmons [13]. The transmission of light along the z direction can be envisaged as plasmon tunneling or hopping. A point source closely located to the surface of the multilayer excites a plas-

monic oscillation at the uppermost metal/dielectric interface. Due to the small thickness of the metal and dielectric layers this excitation induces a similar surface plasmon at the next subjacent interface. The plasmon tunnels from one interface to the next and finally penetrates the whole multilayer material. These coupled surface plasmons are called "multilayer plasmons" in the following. To confirm this interpretation, the magnetic and electric field components of the presented multilayer plasmons are shown in Fig. 4 for three different Bloch wave vectors. These figures represent snapshots of the fields at a particular time. For the Bloch wave with $K_z^B=0$ the field profiles are the same in every period of the multilayer. The magnetic field (left vertical scale) only minimally changes in the dielectric layer, and only slightly more in the silver layer. The overall level remains almost unchanged. The E_x component has a completely different profile and varies between positive and negative values in each period. The field profiles for $K_z^B=\pi/(2R)$ look less symmetric and the determining influence of the Bloch wave vector is clearly visible. Finally the fields for $K_z^B=\pi/R$ show the expected phase shift of π between the fields of adjacent periods. The magnetic field drops to 0 at the center of the silver layers while E_x reaches only a shallow local minimum at a very high level. All field profiles show distinct field concentrations at the interfaces and an exponential decay of the fields away from the interface. This confirms the interpretation of the modes as multilayer plasmons. Furthermore the magnetic field within the dielectric layers keeps its symmetric character, which the modes inherited from their origin as symmetric cavity plasmons.

How does this scheme of multilayer plasmons fit together with the effective medium approximation?

The answer is found by considering wave vector diagrams. In Fig. 5 the wave vector diagrams at two different frequencies are shown. For each frequency the hyperbolic wave vector relationship of the effective medium model (triangles) is compared with the wave vectors of 3 silver/dielectric multilayers. The filling factor of all 3 multilayers is 0.5 so that a comparison with the effective medium is possible. As k_z component of the coupled multilayer plasmons the Bloch wave number K_z^B is taken. To allow a better overview in Figs. 5(a) and 5(c) the extended zone scheme of the multilayer Bloch waves is chosen. It includes several Brillouin zones. The isofrequency curves of the multilayer Bloch waves are the wavy curves. Their periodicity depends on the width of the Brillouin zones which is $\frac{2\pi}{R}$. As the real space period R varies from $R=40$ nm over $R=20$ nm to $R=10$ nm, the width of the Brillouin zones increases from $\frac{2\pi}{40\text{ nm}}=0.157\text{ nm}^{-1}$ over $\frac{2\pi}{20\text{ nm}}=0.31\text{ nm}^{-1}$ to $\frac{2\pi}{10\text{ nm}}=0.63\text{ nm}^{-1}$ for the different multilayers. The first Brillouin zone for every multilayer is centered at $K_z^B=0$ and ranges from $-\pi/R$ to π/R. As k_x appears only squared in all equations, the isofrequency surfaces have the same form for positive and negative k_x, so that the wave vector diagram is mirror symmetric about the k_z axis.

For small wave vectors k_z the isofrequency contours derived from multilayer-Bloch waves and effective medium approximation agree very well [Figs. 5(b) and 5(d)]. This means that the extraordinary waves of the effective medium

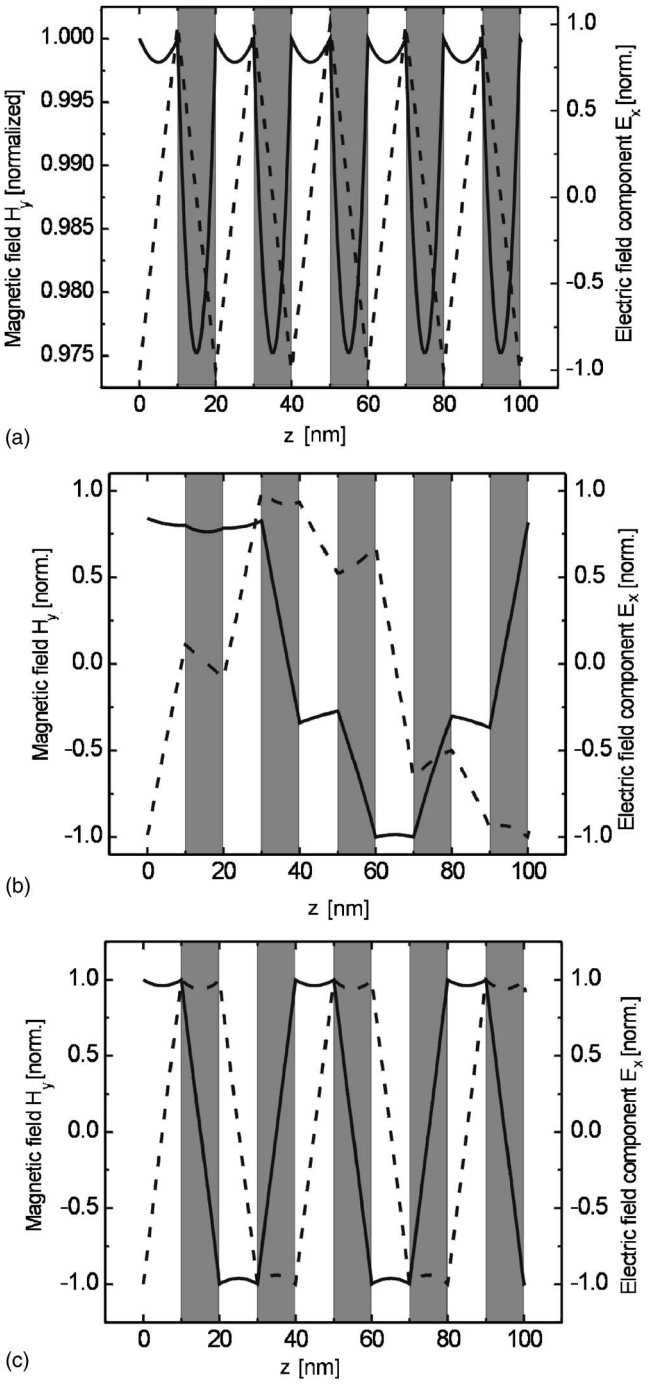

FIG. 4. Field distributions within the multilayer for different wave vector components k_z. (a) Magnetic field H_y (solid curve) and electric field component E_x (dashed) for $k_z=0$. (b) H_y (solid curve) and E_x (dashed) for $k_z=\frac{1}{2}\frac{\pi}{R}$. (c) H_y (solid curve) and E_x (dashed) for $k_z=\frac{\pi}{R}$.

calculation can be identified as multilayer plasmons obtained from the exact calculation. In this way the global picture of extraordinary waves in an effective medium is unified with the local description of multilayer plasmons. For larger k_z however the exact multilayer solutions drop off. This happens at first for the solutions of the multilayer with $R=40$ nm. The corresponding plasmon band has the smallest

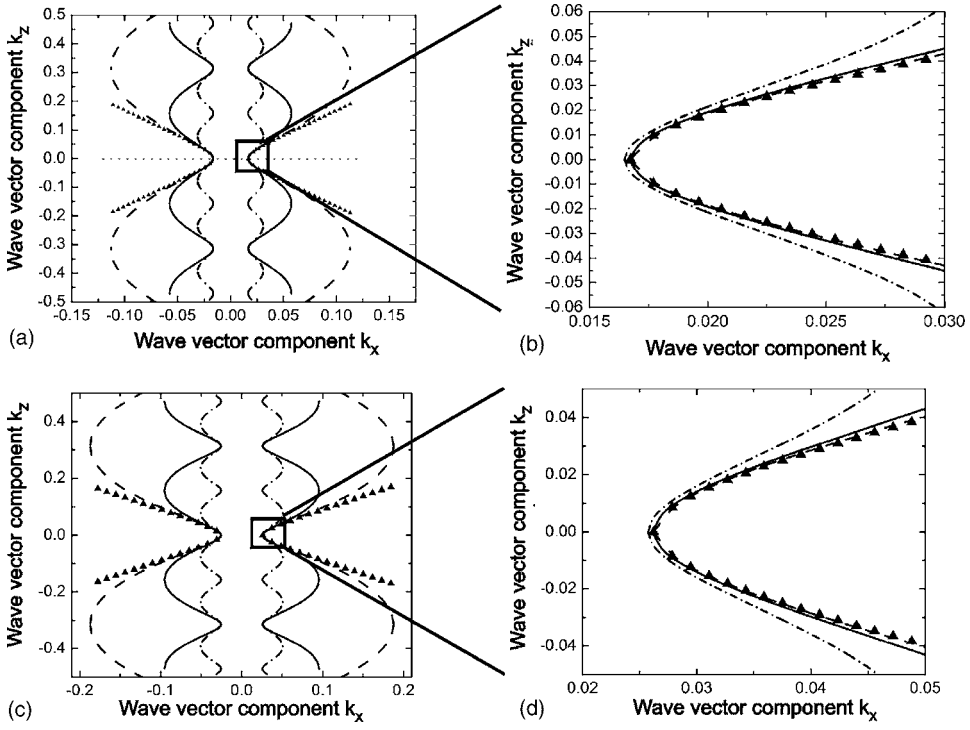

FIG. 5. Wave vector diagrams for silver-dielectric multilayers with a filling factor of $f=0.5$. Solid curves represent wave vectors in structures with $d_{Ag}=10$ nm/$d_{diel}=10$ nm. Dashed and dash-dot curves correspond to wave vectors in multilayers with $d_{Ag}=5$ nm/$d_{diel}=5$ nm and $d_{Ag}=20$ nm/$d_{diel}=20$ nm, respectively. (a) Overview of wave vector dispersion at $\lambda=826$ nm. Triangles mark the wave vectors calculated using the effective medium approximation. (b) Detail of the wave vector diagram at $\lambda=826$ nm revealing the good agreement of effective medium approximation and exact calculation for small k_z. (c) Overview of wave vector dispersion at $\lambda=563$ nm. (d) Detail of ( ) for small k_z.

bandwidth and its upper band edge lies already at $k_x=0.0508$ nm^{-1} ($\lambda_0=563$ nm) or $k_x=0.031$ nm^1 ($\lambda_0=826$ nm). The wave vectors for the multilayer with $R=20$ nm agree over a larger range of k_x quite well with the hyperbolic isofrequency curve of the effective medium. As expected the best agreement over the largest k_x range is achieved with the thinnest layers ($R=10$ nm). The exact multilayer solution coincides exceptionally well with the hyperbolic effective medium solutions up to $k_x \approx 1.2$ nm^{-1} when the multilayer solutions finally drop off. As a rule of thump it can be suggested that the isofrequency curve for the lower half of the plasmon band can be approximated rather well by the effective medium relation.

While the approximate effective medium solutions predict an increase of k_x and k_z ad infinitum, the bandwidth of the exact solutions is limited to the maximum k_x at the upper band limit. Since the layer thicknesses decrease, the upper band limit can be shifted to larger k_x values. However it will always stay finite. This is the primary qualitative difference between the effective medium approximation and the exact multilayer Bloch waves. While the effective medium approximation would allow the propagation of waves with infinitely large k_x, the exact multilayer solution allows only propagating modes up to a certain maximum k_x which depends on the layer thickness.

During the discussion of the effective medium approximation for $\varepsilon_\parallel$ the appearance of resonances was pointed out. For a filling factor of $f=0.5$ this resonance lies in the UV which is far off from the specific wavelengths $\lambda_0=563$ nm and $\lambda_0=826$ nm discussed up to now. However if the filling factor is $f=0.88$ the resonance lies at $\lambda_{0res}=643$ nm so that $\lambda_0=563$ nm lies on the short wavelength side and the resulting effective dielectric constant $\varepsilon_\parallel^{eff}$ at $\lambda_0=563$ nm is negative. This means, that $\varepsilon_\parallel^{eff}$ and $\varepsilon_\perp^{eff}$ are both negative for this wavelength and no propagating modes exist after the effective medium approximation. On the other hand $\lambda_0=826$ nm lies still on the long wavelength side and its $\varepsilon_\parallel^{eff}$ is still positive. Its value increased to $\varepsilon_\parallel^{eff}=41.3$ partly due to the proximity of the resonance.

This situation is compared with the exact multilayer solutions in the wave vector diagrams of Fig. 6. Two multilayer structures with a common filling factor of $f=0.88$ and silver thicknesses of $d_{Ag}=10$ nm and $d_{Ag}=20$ nm are shown. These particular silver thicknesses were chosen to achieve a similar coupling of the plasmons across the silver layers and to allow a comparison with Fig. 5. Contrary to the effective medium approximation, propagating multilayer plasmons exist at $\lambda_0=563$ nm [Fig. 6(a)]. Compared to Fig. 5(d), the wave vector curves are shifted to considerable higher k_x values which seems to be the result of the higher metal content of the structure ($f=0.88$!). As the effective medium approximation does not allow any propagating modes, no hyperbolic curve appears for $\lambda_0=563$ nm. For $\lambda_0=826$ nm the hyperbolic isofrequency curve of the effective medium exists and is compared with the exact multilayer solutions in Fig. 6(b).

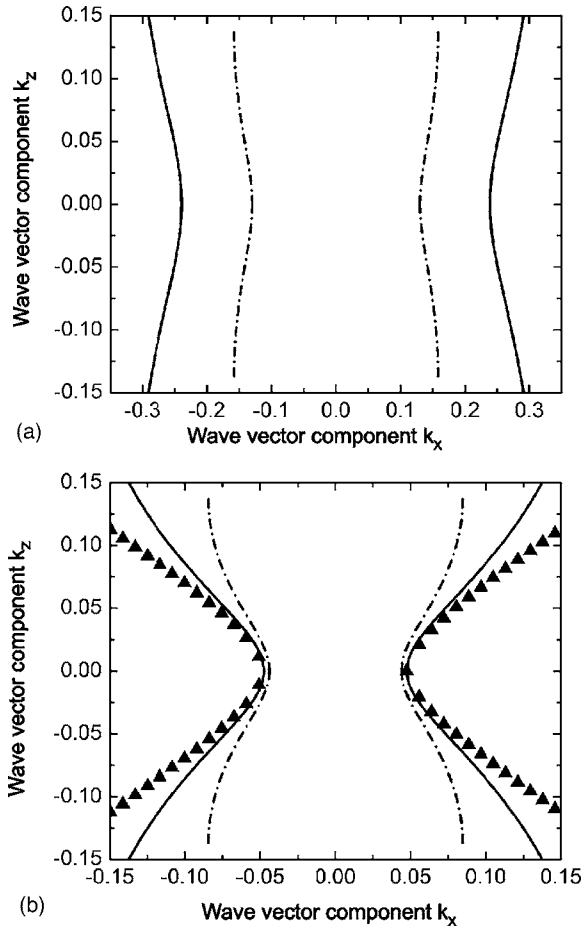

FIG. 6. Wave vector diagrams for silver-dielectric multilayers with a filling factor of $f=0.88$. Solid curves represent multilayers with $d_{Ag}=10$ nm/$d_{diel}=1.36$ nm and dash-dot curves belong to multilayers with $d_{Ag}=20$ nm/$d_{diel}=2.72$ nm. (a) Wave vector dispersion for $\lambda=563$ nm. The effective medium approximation gives negative values for both principal dielectric constants at this wavelength, so that no propagating modes should exist following this approximation. In contrary the exact calculation yields propagating waves represented by the solid and dash-dot curves. (b) Wave vector dispersion for $\lambda=826$ nm. Triangles mark the wave vectors calculated using the effective medium approximation at $\lambda=826$ nm.

For small k_z the hyperbola fits the exact solutions still remarkably well. However the multilayer solutions drop off faster than in Fig. 4(b) and the k_x values are overall larger than in Fig. 5(b).

As the results for effective medium approximation and exact Bloch wave calculation disagree qualitatively for $\lambda_0=563$ nm, one has to conclude that the effective medium approximation fails at this point. The resonance for $\varepsilon_{\parallel}^{\text{eff}}$, which is predicted by the effective medium model, is an artifact of the simple model.

CONCLUSION

In summary it was demonstrated that many interesting optical phenomena, which are normally ascribed to metamaterials with at least partly negative permeability, should also appear in uniaxial metamaterials with an indefinite dielectric tensor and scalar positive permeability. Two principal dielectric constants with different sign are sufficient to create a hyperbolic wave vector relation for the extraordinary waves. This is the basis for many of the discussed phenomena. As an example for such a uniaxial metamaterial a metallodielectric multilayer stack was presented. The exact calculation of the dispersion relation reveals, that extraordinary waves travel as multilayer plasmons through the structure. For small wave vectors (long wavelengths) a very good agreement of effective medium theory (Wiener formulas) and exact calculation is obtained, if the thickness of the layers is about 10 nm. For larger wave vectors the effective medium theory looses its validity as the maximum wave vector component parallel to the layer surfaces is limited. The apparent resonances in the Wiener formulas (effective medium approximation) predicting strong negative and positive dielectric constants do not coincide with the exact calculations and describe the reality wrongly.

As the discussed uniaxial media do not require complex inductive structures to create a negative μ, they are easier to fabricate for short wavelengths such as the visible and infrared spectral range. Since no special LC resonance is required, the spectral range over which these materials keep their properties are much larger than for metamaterials relying on a negative μ. These reasons should ensure strong interest and further thorough investigations of this class of metamaterials.

ACKNOWLEDGMENTS

The author would like to acknowledge interesting discussions with A. Schuchinsky and A. Zayats and the support by the Royal Society.

[1] V. G. Veselago, Sov. Phys. Usp. **10**, 509 (1968).
[2] R. A. Shelby, D. R. Smith, and S. Schultz, Science **292**, 77 (2001).
[3] J. B. Pendry, Phys. Rev. Lett. **85**, 3966 (2000).
[4] R. A. Depine and A. Lakhtakia, New J. Phys. **7**, 158 (2005).
[5] V. M. Shalaev, Opt. Lett. **30**, 3198 (2005).
[6] G. Dolling, D. Enkrich, M. Wegener, C. M. Soukoulis, and S. Linden, Science **312**, 892 (2006).
[7] K. J. Webb and M. Yang, Opt. Lett. **31**, 2130 (2006).
[8] L. Hu and S. T. Chui, Phys. Rev. B **66**, 085108 (2002).
[9] D. Schurig and D. R. Smith, New J. Phys. **7**, 162 (2005).
[10] L. Zhou, C. T. Chan, and P. Sheng, Phys. Rev. B **68**, 115424 (2003).
[11] The real and imaginary part of the refractive index for silver were taken from: Palik, *Handbook of Optical Constants of Solids* (Academic Press, New York, 1984).
[12] A. Yariv and P. Yeh, *Optical Waves in Crystals* (Wiley-Interscience, New York, 2003).
[13] E. N. Economou, Phys. Rev. **182**, 539 (1969).